Bridging Effects of Sulfur Anions at Titanium Oxide and Perovskite Interfaces on Interfacial Defect Passivation and Performance Enhancement of Perovskite Solar Cells

Yang Liu, Hao Sun, Feiyi Liao, Gaocai Li, Chen Zhao, Can Cui, Jun Mei,* and Yiying Zhao*

Cite This: ACS Omega 2021, 6, 34485−34493

Read Online

ACCESS | Metrics & More | Article Recommendations | SI Supporting Information

ABSTRACT: Interfacial defects at the electron transport layer (ETL) and perovskite (PVK) interface are critical to the power conversion efficiency (PCE) and stabilities of the perovskite solar cells (PSCs) via significantly affecting the quality of both interface contacts and PVK layers. Here, we demonstrate a simple ionic bond passivation method, employing Na_2S solution treatment of the surface of titanium dioxide (TiO_2) layers, to effectively passivate the traps at the $TiO_2/Cs_{0.05}(MA_{0.15}FA_{0.85})_{0.95}Pb$-$(Br_{0.15}I_{0.85})_3$ PVK interface and enhance the performance of PSCs. X-ray photo-electron spectroscopy and other characterizations show that the Na_2S treatment introduced S^{2-} ions at the TiO_2/PVK interface, where S^{2-} ions effectively bridged the TiO_2 ETL and the PVK layer via forming chemical bonds with Ti atoms and with uncoordinated Pb atoms and resulted in the reduced defect density and improved the crystallinity of PVK layers. In addition, the S^{2-} ions can effectively enlarge the grain size of the PVK layers. The average PCE of solar cells is improved from 15.77 to 19.06% via employing the Na_2S-treated TiO_2 layers. This work demonstrates a simple

and facile interface passivation method using ionic bond passivation to afford high-performance PSCs. The bridging effect of S^{2-} ions may inspire the further exploration of the ionic bond passivation and sulfur-based passivation materials.
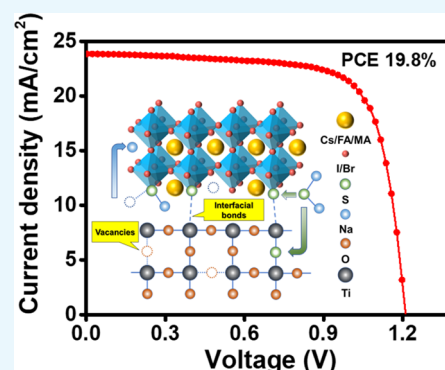
INTRODUCTION

Organic−inorganic hybrid halide perovskite (PVK) materials have attracted enormous interest in solar cell applications, and the power conversion efficiency (PCE) of single-junction perovskite solar cells (PSCs) has improved from 3.8 up to 25.5% in 2021[1,2] due to their extraordinary optoelectronic properties such as the suitable band gap, large absorption coefficient, and high carrier mobility.[3−5] However, further improvements of PSC efficiency and stability are limited by the defects in the PVK layers and at the PVK/electrode interfaces, which could cause serious charge recombination and thus lower the short-circuit current.[6] Compact titanium dioxide (TiO_2) is the most widely used electron transport layer (ETL) in PSCs for its suitable energy level alignment, easy fabrication, and good interface quality. However, the severe hysteresis effect and the TiO_2/PVK interface of TiO_2-based PSCs limit their further applications and tremendous attention has been devoted to the surface passivation in the TiO_2/PVK interface.

There are two general strategies to passivate the ETL/PVK interface including the covalent bond passivation and the ionic bond passivation. The most well-studied covalent bond passivation is the Lewis acid−base chemistry method, based on the formation of covalent bonds between Lewis adducts and defects, which leads to the effective passivation of the interface defects and the improvement of the performance and stability of PSCs. Peng et al. introduced a double-side polymer

poly(methyl methacrylate) (PMMA) at TiO_2/PVK and PVK/spiro-OMeTAD interfaces and finally improved the PCE of PSCs to 20.8% with an impressive open-circuit voltage (V_{oc}) of 1.22 V.[7] Characterizations of the PVK−PMMA molecular interface show that carbonyl (C=O) groups in PMMA can aid in the reduction of Pb^{2+} defect density at the ETL/PVK and PVK/HTL interfaces. Hou et al. effectively passivated ETL/PVK interface traps via hydrogen-bonding interactions (N−H/I), where the dopamine self-assembled monolayer on the SnO_2 ETLs improved the carrier transport and significantly improved the PCEs of the corresponding PSCs from 14.05 to 16.65%.[8] Wang et al. demonstrated PSCs with stabilized PCEs of 22.6% via introducing a dopamine self-assembled monolayer on the top of the SnO_2 ETL, which effectively passivate the surface antisite Pb (lead) defect by means of the assisted primary C=O binding.[9] Most recently, Zhou demonstrated a decreased open-circuit voltage deficit from 0.47 to 0.39 V with a stabilized efficiency of 22.99% by permeating a fluorinated perylene-tetracarboxylic diimide
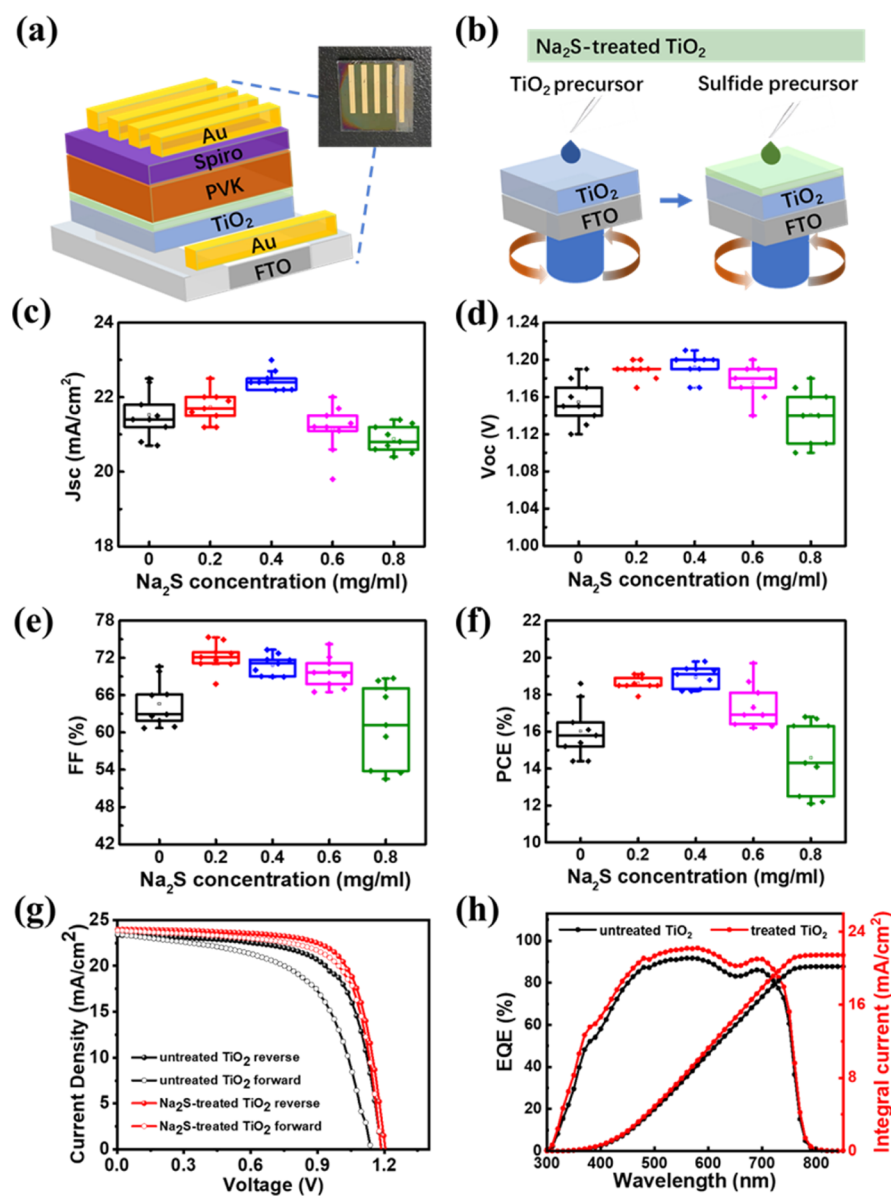
Figure 1. PSCs with TiO_2 layers treated with different Na_2S solutions. (a) Diagram of the device structure and photograph of PSCs; (b) schematic diagram of the fabrication process of Na_2S surface treatment of the compact TiO_2 layer; (c) short-circuit current density J_{sc}, (d) open-circuit voltage V_{oc}, (e) FF, and (f) PCE of PSCs with TiO_2 layers treated with Na_2S solutions of different concentrations. (g) $J-V$ curves of the devices with and without Na_2S treatment under both reverse-scan and forward-scan directions and (h) EQE spectra of PSCs with and without the Na_2S treatment of 0.4 mg/mL.

derivative on the PVK layer to passivate under-coordinated Pb^{2+} defects.[10] Chen utilized poly(propylene glycol)bis(2-aminopropylether) (PEA) additive in PVK layers, which interacted with the lead ions and considerably passivated surface and bulk defects.[11] Cai used carbonyl groups in 2,2-difluoropropanediamide to form chemical bonds with Pb^{2+} and passivate under-coordinated Pb^{2+} defects in PVK layers.[12] Besides, reduced graphene oxide-based materials with oxygen-based hydroxyl ($-OH$) groups and other Lewis bases containing amines (such as $-NH_2$) or nitrogen functionalities have also been proved of effective passivation.[13−16] Meanwhile, chemical bonds reduced the crystallization rate, producing high-quality PVK films with fewer defects.[12]

Ionic bond passivation includes cation passivation and anion passivation. Cationic substances including metal ions and organic molecules form ionic bonds and other electrostatic

interactions with negatively charged traps (such as uncoordinated I^-, PbI_3^-, and MA^+ vacancies) in PVK materials, proving to be effective.[17] Metal ions were reported by Bi et al. for the first time that can effectively passivate defects at grain boundaries of PVK layers.[18] Na^+ ions on the PTAA [poly(bis(4-phenyl)(2,4,6-trimethylphenyl)amine)] HTL were found to diffuse into the grain boundaries of PVK layers, resulting in a lower defect density and a longer photoluminescence (PL) lifetime. Since the size and equivalent charge of Na^+ are similar to those of MA^+, the Na^+ ions fill MA vacancies at grain boundaries and thus reduce negatively charged trap densities. Abdi-Jalebi et al. reported an impressive high internal PL quantum yield (larger than 95%) by adding potassium iodide (KI) to the $Cs_{0.06}FA_{0.79}MA_{0.15}Pb(I_{0.85}Br_{0.15})_3$ PVK precursor, resulting in the accumulation of the K^+ ions at the surface and grain boundaries to passivate those extended
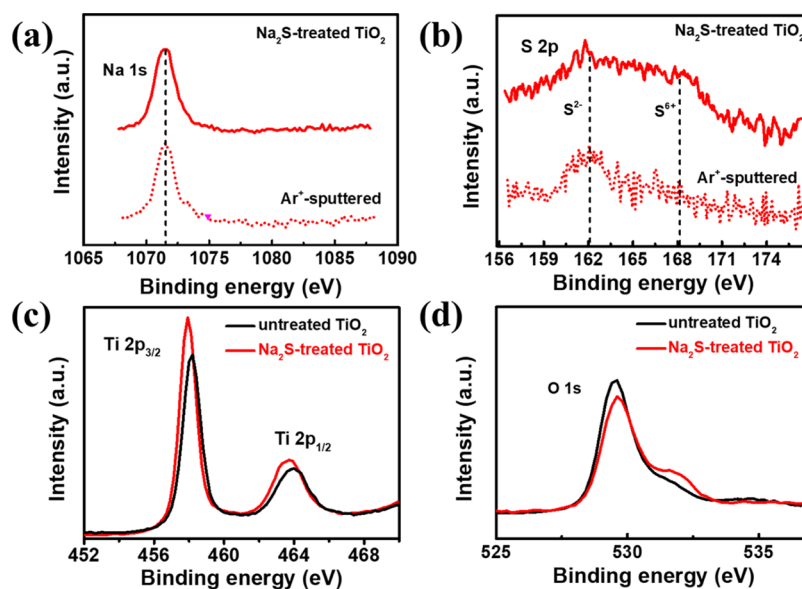
Figure 2. XPS spectra (a) of Na 1s peaks and (b) S 2p peaks of the Na$_2$S-treated TiO$_2$ layer and the same sample sputtered with argon ions for 5 min and XPS spectra of (c) Ti 2p peaks and (d) O 1s peaks of the compact TiO$_2$ layer with and without Na$_2$S treatment.

defects.[19] Beyond alkali metal ions including Cs$^+$ and Rb$^+$, Cu^{2+} and Ag$^+$ are also reported to be capable of effective passivation.[20−23] Small organic molecules owning ammonium functionalities such as butylammonium (BA$^+$), octylammonium (OA$^+$), phenylethylammonium (PEA$^+$), and diammonium derivatives have also been explored for their ability to enhance device performance and suppress trap-induced recombination.[24−27] However, there are only a few works on the anion passivation of insufficiently coordinated Pb^{2+} ions and halide vacancies. Reported anions for the trap passivation of PSCs include chloride ions (Cl$^−$) and sulfide ions (S$^{2−}$). Pool et al. reported that the Cl$^−$ ions show effective passivation on the traps at interfaces and/or grain boundaries and also enlarge the grain size of PVK layers.[28] Wang et al. reported a solution-processing method to form strong Pb−Cl and Pb−O bonds between PVK films and chlorinated graphene oxide layers to stabilize the heterostructure.[29] Chen and Cao et al. also discussed the bonding between S atoms with Pb atoms and demonstrated that the bonding is significantly effective for high-performance PSCs.[30,31] Sun achieved a PCE as high as 21.25% with an impressive high V_{oc} of 1.22 V by doping Na$_2$S into TiO$_2$ layers, demonstrating the significant effect of S$^{2−}$ and Na$^+$ ions.[32] However, the doping method is limited by the solubility of Na$_2$S in the TiO$_2$ precursors and the high-temperature calcination process of the TiO$_2$ layer is not compatible with the flexible PSC fabrication process. In addition, we were curious whether the Na$^+$ and S$^{2−}$ ions on the surface of TiO$_2$ layers have better effects than those in the TiO$_2$ layers. In addition, it is still unclear whether the crystal grain enlargement of PVK grains is caused by the surface roughness or the S$^{2−}$ ions on the surface of TiO$_2$ layers. Therefore, it is necessary to come up with other methods to effectively introduce Na$^+$ and S$^{2−}$ ions on TiO$_2$ surfaces and is also very important to understand the interface passivation mechanism and explore the new interface passivation material.

Herein, we demonstrate that a simple Na$_2$S treatment of the TiO$_2$ surfaces can effectively passivate the defects at the TiO$_2$/PVK interface and improve the quality of PVK layers, leading to an enhancement of the solar cell performance. The TiO$_2$ layers were spin-coated with Na$_2$S solution before the PVK layer deposition, and PSCs with a typical structure of fluorine-doped tin oxide (FTO)/TiO$_2$/Cs$_{0.05}$(MA$_{0.15}$FA$_{0.85}$)$_{0.95}$Pb-(Br$_{0.15}$I$_{0.85}$)$_3$/Spiro-OMeTAD/Au were fabricated to investigate the effect on the surface passivation and device performance. Experimental results show that this simple Na$_2$S treatment can effectively introduce S$^{2−}$ ions on the surface of TiO$_2$ layers and improve the average efficiency from 15.77 to 19.06%. S$^{2−}$ ions can improve the crystallinity of PVK layers grown on the Na$_2$S-treated TiO$_2$ substrate, evidenced by a higher PL intensity, a longer photogenerated carrier lifetime, and a larger grain size. Space-charge-limited current (SCLC) and J−V curves indicate that devices with the Na$_2$S treatment show the reduced carrier recombination loss at the TiO$_2$/PVK interface and the suppression of interface recombination. This simple method will inspire the exploration of sulfide-based interface passivation in the research community of PSCs.

RESULTS AND DISCUSSION

PSCs with the typical structure of FTO/TiO$_2$/(Na$_2$S)/PVK/Spiro-OMeTAD/Au shown in Figure 1a were prepared to investigate the effects of Na$_2$S treatment on device performances. The Na$_2$S treatment includes the conventional spin-coating process and the postannealing process right after the annealing of TiO$_2$ layers, as shown in Figure 1b. Ethanol solutions of sodium sulfide with concentrations from 0.2 to 0.8 mg/mL were prepared as the precursor solution. Ten solar cells of each condition were tested under the AM 1.5 solar spectrum, and the device performances are shown in Figure 1c−f and details are listed in Table S1. It can be seen that the PCE first increases and then decreases with the increase of the Na$_2$S concentration. The similar trend is also found in the parameters of J_{sc}, V_{oc}, and fill factor (FF). The devices prepared with a Na$_2$S solution of 0.4 mg/mL have the best performance, with an average PCE improvement from 15.77 to 19.06%, the average short-circuit current improvement from 21.39 to 22.39 mA/cm^2, an average opening voltage increase from 1.149 to 1.191 V, and the average FF increase from 62.80 to 71.14%. The device performance degradation at a higher Na$_2$S
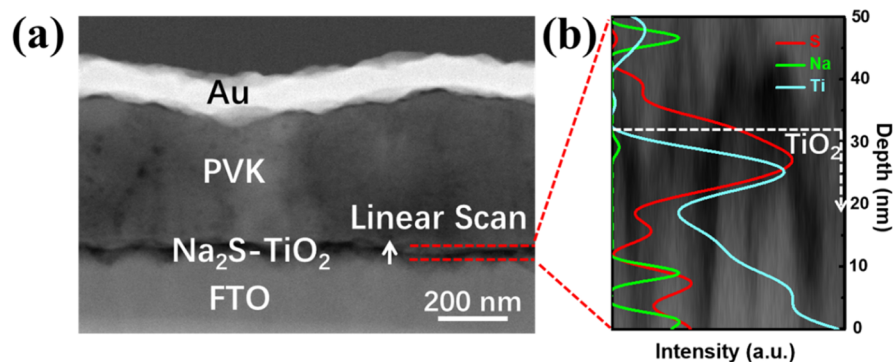
Figure 3. (a) HAADF-STEM image of the cross-section of PVK films deposited on the TiO$_2$ layer with Na$_2$S treatment and (b) EDS mapping in a linear scan mode through the cross-section of FTO/TiO$_2$/PVK stack.
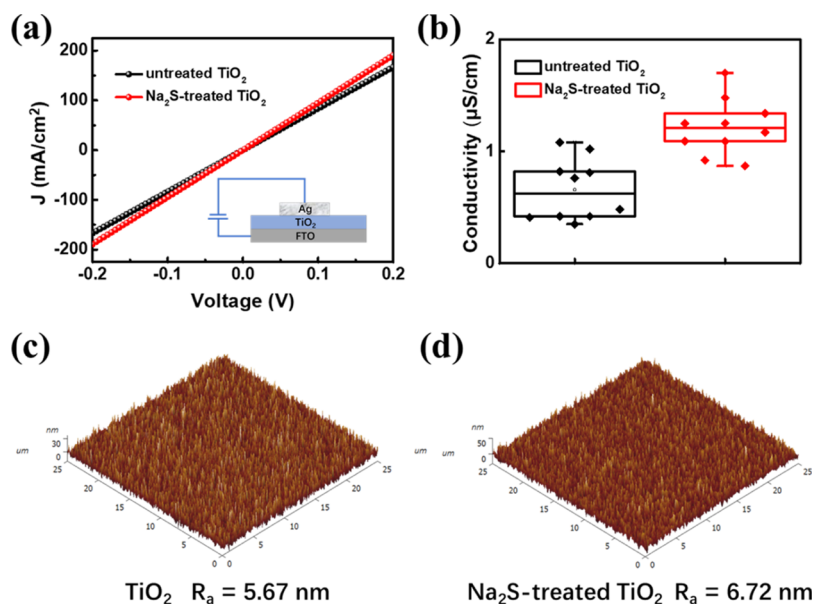
Figure 4. Characterization of TiO$_2$ layers with and without Na$_2$S treatment. (a) $J-V$ characteristic curves; (b) box diagrams of conductivity measurements of two samples; and AFM images [three-dimensional (3D)] of TiO$_2$ layers without (c) and with (d) Na$_2$S treatment.

concentration is probably caused by the rough surface and the Na$_2$S residue on the surface of TiO$_2$ layers, as shown in Figure S1, which severely deteriorate the quality of the following PVK layer. Therefore, the surface treatment of TiO$_2$ layers with a proper Na$_2$S concentration can effectively improve the PSC performance, and the optimal concentration is 0.4 mg/mL in this work.

Figure 1g shows the $J-V$ curves of PSCs measured under both reverse-scan and forward-scan directions with or without Na$_2$S treatment. Obviously, devices with the Na$_2$S treatment have smaller hysteresis. According to Shi,[6] the hysteric index (HI) factor of PSCs with the Na$_2$S-treated TiO$_2$ layers dropped from 0.156 to 0.061. The external quantum efficiency (EQE) of PSCs with the Na$_2$S-treated TiO$_2$ layers was higher than that of PSCs without treatment in the wavelength range of 300−900 nm, as shown in Figure 1h, indicating that the device with Na$_2$S treatment has an effective charge collection. The integrated current density from EQE is smaller than that from the $J-V$ measurements, probably due to the differences in the light sources used.[33] The light storage stability of PSCs with and without the Na$_2$S treatment in the ambient under continuous sunlight (1 sun) is shown in Figure S2. The ambient humidity during the test is 86%, and the temperature

of the device surface irradiated by sunlight is 48 °C. After a continuous radiation of AM 1.5G for 5 h, the unpackaged PSCs with the Na$_2$S-treated TiO$_2$ layers demonstrate a higher light storage stability in the high humidity ambient, with a 24% drop of the initial efficiency, compared with the 36% efficiency drop of the untreated devices. In conclusion, the Na$_2$S treatment of the TiO$_2$ surface can effectively reduce the hysteresis behavior and improve the charge collection efficiency and the stability of PSCs.

X-ray photoelectron spectroscopy (XPS) characterizations were conducted to verify the existence and the chemical bond states of Ti, O, Na, and S ions on TiO$_2$ layers with and without Na$_2$S treatment. The peaks of C 1s at 284.6 eV were used to calibrate the spectra. The characteristic peaks of Na$^+$ 1s at 1071.4 eV and S^{2-} 2p at 162.8 eV can be seen in the XPS spectra of TiO$_2$ layers with Na$_2$S treatment in Figure 2a,b, respectively. The corresponding peaks cannot be seen in the XPS spectra of untreated TiO$_2$ layers shown in Figure S3. Meanwhile, the characteristic peaks of S^{6+} 2p at 168 eV are also shown in the XPS spectra, which were probably formed by the oxidation of S^{2-} during the postannealing process.[34] XPS characterizations were also performed on the Na$_2$S-treated TiO$_2$ layers after a 5 mins' sputtering of Ar$^+$ ions to further
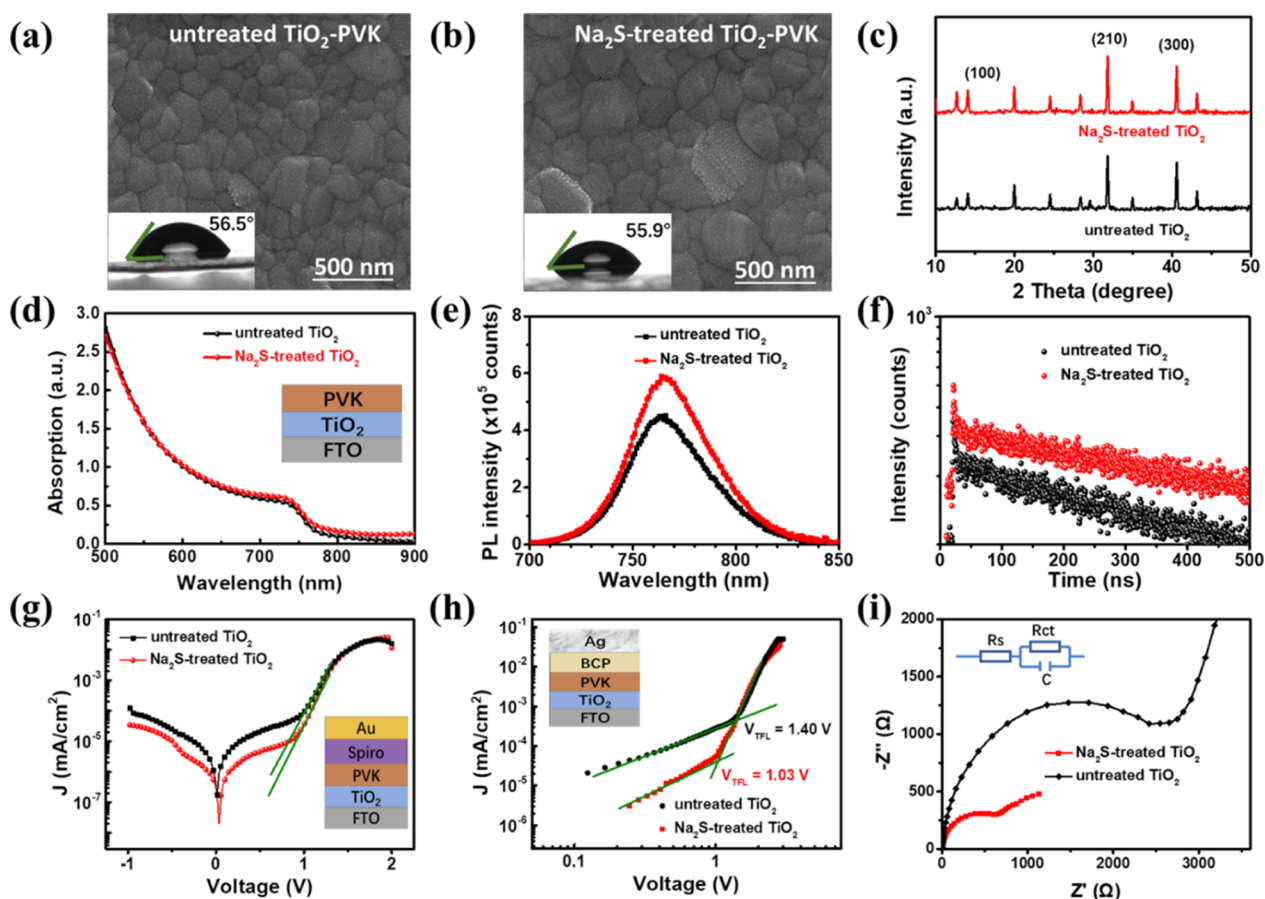
Figure 5. Characterizations of PVK layers and TiO$_2$/PVK interfaces with and without Na$_2$S treatment. Scanning electron microscopy (SEM) images of PVK layers on TiO$_2$ substrates (a) without and (b) with Na$_2$S treatment, with the surface contact angles of water as the insets; (c) X-ray diffraction (XRD) diagrams, (d) UV−visible absorption spectra, (e) PL spectra, and (f) time-resolved PL (TRPL) spectra of the PVK layers on TiO$_2$ substrates with/without Na$_2$S treatment; (g) J−V curves of devices on TiO$_2$ substrates with/without Na$_2$S treatment under the dark; (h) J−V curves of electron-only devices on TiO$_2$ substrates with/without Na$_2$S treatment; and (i) Nyquist plot of electrical impedance spectroscopy (EIS) of devices on TiO$_2$ substrates with and without Na$_2$S treatment. Inset: the device structure in the test.

investigate the elemental distribution of the Na$^+$ and S^{2-} ions. The existence of Na$^+$ 1s peaks and S^{2-} 2p peaks in the sputtered samples shown in Figure 2a,b implies that both Na$^+$ and S^{2-} ions diffuse into the TiO$_2$ films. Figure 2c,d shows the XPS spectra of Ti 2p and O 1s peaks of TiO$_2$ films with and without Na$_2$S treatment. It can be seen very clearly that the Ti 2p peaks at 458.2 and 464.0 eV of the typical Ti−O bonds in untreated TiO$_2$ layers[35] shift slightly to the direction of low binding energy in the spectra of the TiO$_2$ layers with Na$_2$S treatment. This result indicates that S^{2-} ions may form chemical bonds with Ti^{4+} via substituting oxygen atoms or filling the oxygen vacancies,[36] resulting from the lower electronegativity of S^{2-} ions compared with that of O^{2-} ions. From Figure 2d, it can be observed that the peak height of adsorbed oxygen at 531.8 eV is higher and that of lattice oxygen peaks at 530.2 eV is lower in the TiO$_2$ layer with Na$_2$S treatment, which implies the existence of S^{2-} ions on the Na$_2$S-treated TiO$_2$ layers. All these results prove that Na$^+$ and S^{2-} ions are successfully introduced into the compact TiO$_2$ layers, and the S^{2-} ions probably form the chemical bonds with Ti^{4+} ions.

The elemental scanning in the linear mode through the cross-section of the FTO/TiO$_2$/PVK structure under high-angle annular dark-field scanning transmission electron microscopy (HAADF-STEM) was carried out to further

investigate the spatial distribution of Na and S ions in the TiO$_2$ layers and TiO$_2$/PVK interfaces. As shown in Figure 3a,b, the region of TiO$_2$ layers can be roughly determined by the signal of Ti elements. Due to the small atomic numbers of Na elements and S elements, obvious background noise may appear in the energy-dispersive X-ray spectroscopy (EDS) scanning. It is interesting to note that the EDS intensity of Na atoms is lower and the distribution profile is more uniform compared with that of the S atoms. The elemental intensity (counts of the fingerprint EDS signal) profile indicates that elements S and Na are present in both TiO$_2$ layers and PVK layers. We speculate that S ions at the TiO$_2$/PVK interface may diffuse into the PVK layers and form bonds with Pb, while Na could diffuse into both PVK and TiO$_2$ layers. Correlating the XPS results in Figure 1c, it can be concluded that part of S^{2-} ions also forms bonding with Ti^{4+}, and the bilateral bonds of S ions enhance the chemical binding at the TiO$_2$/PVK interface. The appearance of the Na signal in the PVK layer indicates that alkali-metal elements can diffuse into the PVK layer and passivate the grain boundaries.[18]

The electron-only devices with the structure of FTO/TiO$_2$/ (Na$_2$S)/Ag shown as the inset of Figures 4a and S4 were fabricated to investigate the effect of Na$_2$S treatment on the electrical properties of TiO$_2$ layers. The J−V characteristic curves of both structures measured under the dark are shown

in Figure 4a, and the slopes stand for the conductivity of the samples. The conductivity of TiO_2 layers was calculated from the linear fitting of the curves in Figure 4a, and the box diagrams are shown in Figure 4b. The conductivity of TiO_2 layers with Na_2S treatment is higher than that of the untreated samples, indicating that the improved conductivity of TiO_2 layers resulted from the introduction of Na^+ ions. The fact that the conductivity improvement of TiO_2 layers is not as significant as that in the previous work is probably caused by the smaller Na atoms introduced by this spin-coating method.[32] This result is consistent with the results in Figure 3 and the previous reports that alkali-metal ions can improve the TiO_2 film conductivity.[18,32] Figure 4c,d shows the atomic force microscopy (AFM) images of the surface of TiO_2 layers with and without Na_2S treatment, where the surfaces of both samples are very smooth. The TiO_2 layer with Na_2S treatment has an average roughness (Ra) of 6.72 nm, which is almost the same as that of the TiO_2 layer, indicating almost no effect of Na_2S treatment on the morphology of the TiO_2 layer.

To fully understand the effects of Na_2S treatment, systemic characterizations of the TiO_2/PVK interfaces and the following PVK layers were conducted. From the SEM images shown in Figure 5a,b, we can see that the crystal grain size of the PVK layers on the TiO_2 substrates with Na_2S treatment is larger than that on the untreated TiO_2 substrates. The larger grain size leads to fewer grain boundaries which are beneficial to carrier transport.[37,38] Meanwhile, the contact angle of water on the TiO_2 substrates with Na_2S treatment is similar to that of the untreated TiO_2 substrates, indicating that the Na_2S treatment will not affect the hydrophobicity of the TiO_2 substrates. It can be concluded that the larger grain sizes of the PVK layer probably are not caused by the hydrophobicity of the substrate in this work[39] but the bonding between S atoms and Pb atoms.[32]

XRD characterization of PVK layers on different TiO_2 substrates was conducted to illustrate the influence of Na_2S treatment on the crystallinity of the PVK layers. It can be seen from the XRD diagrams in Figure 5c that the positions of all the diffraction peaks in both samples are the same. Main diffraction peaks at 14.1, 31.8, and 40.6° can be identified as those of the (100) (210) (300) crystal plane of the cubic PVK, respectively. There are no new characteristic peaks or shift of the peak position, indicating that the Na_2S treatment does not change the crystal structure or the phase of the PVK layer. The peak intensity of the (100) crystal plane is enhanced in the samples treated with the Na_2S solution of 0.4 mg/mL, indicating that the crystal alignment along the (100) crystal plane is improved, and the Na_2S treatment is beneficial to improve the crystallinity of the PVK.

Optical properties of PVK layers grown on both TiO_2 substrates were characterized and are shown in Figure 5d−f. Figure 5d shows the UV−visible absorption spectra of the PVK films on both TiO_2 substrates. There is no obvious difference except the slight shift of the absorption edge in the light absorption spectra of PVK films on both samples. The absorption edges of PVK grown on TiO_2- and Na_2S-treated TiO_2 are 787.7 and 785.5 nm, respectively. The calculated band gaps of PVK grown on TiO_2- and Na_2S-treated TiO_2 are 1.574 and 1.579 eV, respectively, indicating that Na_2S treatment has little effect on the energy band structure of the PVK layer. From the PL spectra of both samples shown in Figure 5e, it can be seen that the PVK film grown on the Na_2S=treated TiO_2 substrate exhibits a stronger PL emission,

indicating a better crystal quality. From the TRPL spectra of both samples shown in Figure 5f, it can be seen that the PVK film grown on the Na_2S-treated TiO_2 film exhibits a longer carrier lifetime (656 ns vs 464 ns), which may result from a reduced nonradiative recombination. All these results show that the Na_2S treatment improves the crystal quality of the PVK layers on the TiO_2 substrates. The dark current−voltage characteristic curves of PVK solar cells on different substrates were measured and are shown in Figure 5g to investigate the influence of the Na_2S treatment on the internal loss of carriers. The dark current can be written as the following equation[40]

$$J = J_0 \left[\exp\left(\frac{qV}{nkT} \right) - 1 \right]$$

where J_0 is the reverse saturation current density, q is the amount of charge, V is the voltage, n is the ideality factor, k is the Boltzmann constant, and T is the temperature. The reverse saturation current can be obtained from the intersection point by fitting the exponential region of the I−V curves with a tangent. The J_0 of the PSC devices is reduced from 1.498×10^{-16} to 6.882×10^{-18} mA/cm^2, with the introduction of the Na_2S treatment. The decrease of the J_0 indicates the reduction of the carrier recombination loss at the TiO_2/PVK interface, which is beneficial to the improvement of the open-circuit voltage and the short-circuit current of the device.[40]

SCLC measurements of electron-only devices with a structure of FTO/TiO_2/(Na_2S)/PVK/BCP/Ag were performed to investigate the trap density at the TiO_2/PVK interface and PVK layers. The J−V curves are shown in Figure 5h, and the trap filling limit voltage (V_{TFL}) was obtained from the intersection point.[41] The fittings of the curves show that the V_{TFL} values of the TiO_2 and Na_2S-treated TiO_2 devices are 1.40 and 1.03 V, respectively. The corresponding trap state densities of the device are 2.15×10^{18} and 1.58×10^{18} cm^{-3}, indicating that the Na_2S treatment effectively passivates the traps.

Besides, the EIS measurements were performed under the dark to investigate the effects of Na_2S treatment on the charge transfer at the interfaces. The Nyquist plots of PSCs fabricated on TiO_2 substrates with and without Na_2S treatment are shown in Figure 5i. The equivalent circuit diagram of the devices used to fit the plot is illustrated in the inset of Figure 5i, where R_s is the sheet resistance of electrodes and R_{ct} is the charge-transfer resistance of the TiO_2/PVK interface. The fitted R_{ct} value of the control device is 2955 Ω and that of the device with a Na_2S interfacial layer is 886 Ω. A smaller semicircle suggests a reduced resistance R_{ct}, which means a suppressed recombination at the interface.[42] It can be concluded that the Na_2S-treated TiO_2 layer has a better interface for charge transfer.

Correlating with the above experimental results and discussion, we can summarize the mechanism of Na_2S treatment at the TiO_2/PVK interface in Figure 6. Na_2S treatment can successfully introduce Na^+ and S^{2-} at the TiO_2/PVK interface, where S^{2-} ions form bonds with Ti^{4+} via substituting the oxygen atoms or filling the oxygen vacancies in the TiO_2 layer and anchor-uncoordinated Pb atoms in the PVK layer, leading to the effective ionic bond passivation of interfacial defects, improved crystallinity of PVK layers, and the enhanced PSC performance.[18,20,30,31] Meanwhile, Na^+ ions diffuse into the PVK layer and the TiO_2 layer, resulting in the defect passivation at the grain boundary of PVKs and the
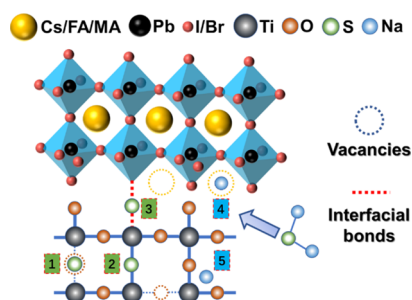
Figure 6. Schematic diagram of the mechanism of Na_2S at the ETL/PVK interface.

improved conductivity of the TiO_2 layer.[18] Compared with the doping method reported in the previous work, the spin-coating method is less effective in introducing Na^+ ions into the TiO_2 layers, which can improve the conductivity of TiO_2 layers and thus enhance the device performance.

CONCLUSIONS

In summary, we demonstrated a simple and effective S^{2-} ionic bond passivation method to reduce defect densities and the corresponding recombination losses at TiO_2/PVK interfaces and in $Cs_{0.05}(MA_{0.15}FA_{0.85})_{0.95}Pb(Br_{0.15}I_{0.85})_3$ solar cells. The passivation method is to treat the TiO_2 surface via spin-coating the Na_2S precursor solution, followed by a postannealing process. XPS and other characterizations indicate that S^{2-} ions can be effectively introduced at the TiO_2/PVK interface and may function as anchoring sites for Pb^{2+} in the PVK layer, resulting in reduced defect densities both at the TiO_2/PVK interface and in the PVK layer, enlarged PVK grain sizes, and inhibited nonradiative recombination. At the optimal Na_2S precursor solution of 0.4 mg/ml, the efficiency of the best device has been improved to 19.8%. Compared with the doping method reported in the previous work,[32] the spin-coating method is less effective in introducing Na^+ ions into the TiO_2 layers and thus the smaller improvement in device performance. Our work on the bridging effects of S^{2-} ions may inspire the further exploration on the interface passivation of the ETL/PVK interface and performance enhancement of PSCs.

EXPERIMENTAL SECTION

Solution Preparation. The TiO_2 precursors were prepared by dissolving 250 μL of tetrabutyl titanate (Sigma-Aldrich) and 25 μL of hydrochloric acid (Kelong) in 3 mL of absolute ethyl alcohol (Aladdin). The Na_2S precursors were prepared by dissolving Na_2S (Aladdin) in absolute ethyl alcohol (Aladdin) according to the concentration of Na_2S. The $Cs_{0.05}(MA_{0.15}FA_{0.85})_{0.95}Pb(Br_{0.15}I_{0.85})_3$ PVK precursor solution consisting of 31.6 mg of cesium iodide (CsI, Alfa Aesar), 19.6 mg of methylammonium bromide (MABr, Lumtec), 67.2 mg of lead bromide ($PbBr_2$, Sigma-Aldrich), 166.6 mg of formamidinium iodide (FAI, luminescence), and 470.2 mg of lead iodide (PbI_2, Sigma-Aldrich) was dissolved in a mixture of 600 μL of dimethylformamide (Sigma-Aldrich) and 400 μL of dimethyl sulfoxide (Sigma-Aldrich) and kept stirring overnight at room temperature in the glovebox. The spiro-OMeTAD solution precursors were prepared by mixing 28.8 μL of 4-*tert*-butylpyridine (Sigma-Aldrich), 17.5 μL of Li-TFSI solution [Li-TFSI (520 mg, Sigma-Aldrich) in acetonitrile (1 mL, Alfa Aesar)], 60 μL of Co (III) TFSI salt solution (FK209 Co (III)

TFSI salt (100 mg, luminescence) in acetonitrile (1 mL, Alfa Aesar), and 72.3 mg of 2,2′,7,7′-tetrakis[*N*,*N*-di(4-methoxyphenyl)amino]-9,9′-spirobifluorene(spiro-OMeTAD, luminescence) in chlorobenzene (1 mL, Alfa Aesar) and kept stirring overnight at room temperature in the glovebox. The BCP (0.5 mg, J&K) was dissolved in absolute ethyl alcohol (1 mL, Aladdin).

Device Fabrication. The FTO glass (sheet resistance = 7 Ω sq^{-1}) after washing by detergent, deionized water, acetone, and isopropanol, respectively, in an ultrasonic cleaner for 20 min was dried with a nitrogen gun and treated with UV−ozone for 15 min. The TiO_2 compact layers were prepared by spin-coating the TiO_2 precursor solution onto the FTO substrates at 5000 rpm for 30 s in air. Then, the samples were preannealed at 120 °C for 20 min on the hot plate and then heated in the muffle oven at 450 °C for 1 h to form the c-TiO_2 layers. For the Na_2S-coated samples, Na_2S precursor solutions were coated onto the compact-TiO_2 layers at 5000 rpm for 30 s in air and then annealed at 120 °C for 20 min on the hot plate to form the Na_2S interfacial layers.

All samples were treated with UV−ozone for 15 min before the PVK deposition process, and PVK layers were prepared by a one-step process in a glovebox. The FTO/c-TiO_2/(Na_2S) substrates were spin-coated at 500 rpm for 5s and 5000 rpm for 50 during the spin-coating process of PVK layers, and 50 μL of chlorobenzene (Alfa Aesar) was injected onto the spinning substrate constantly. Then, the samples were annealed at 150 °C for 10 min on a hot plate. The Spiro-OMeTAD precursor was then deposited on the PVK layers via spin-coating at 5000 rpm for 50 s. At last, 80 nm thick Au electrodes were deposited on the top Spiro-OMeTAD layers using vacuum thermal evaporation.

Characterization. The $I-V$ measurements and stability test were performed using a Keithley 2400 digital source meter under simulated sunlight from a Newport 94123A solar simulator matching the AM 1.5G irradiation (100 mW cm^{-2}). The devices were measured from 1.4 to −0.2 V at a scan rate of 10 mV/s. XPS was carried out on PHI 5000 Versa Probe III. EQE was measured by Enlitech QE-R3011. UV-absorption spectra were recorded using a Youke UV-1901 UV−vis spectrometer. AFM scans were obtained by Bruker Dimension Edge. STEM was performed by an FEI Titan Themis (300 kV). The contact angle measurement was carried out by a contact angle meter (OSA25, Kruss). SCLC and conductivity were tested using a Keithley 2400 digital source meter. Ultraviolet photoelectron spectroscopy (UPS) was performed using a UPS system (Kratos, Axis Ultra) using HeI radiation of 21.22 eV.

XRD patterns were obtained using an EMPYREAN four-circle diffractometer operated at 40 kV and 30 mA at a scan rate of 20° per minute. SEM images were obtained using a field-emission scanning electron microscope (FEI inspect) at an acceleration voltage of 8 kV. Steady-state PL and TRPL were measured using Edinburgh Instruments, FLS 920 equipped with a light source with an excitation wavelength of 375 nm. EIS plots were measured using a CorrTest Electrochemical Workstation under dark conditions.

ASSOCIATED CONTENT

ⓢ Supporting Information

The Supporting Information is available free of charge at https://pubs.acs.org/doi/10.1021/acsomega.1c04685.

Fabricated device and related characterization; performance parameters of PSCs on TiO$_2$ layers modified with different methods; detailed experimental data of actual devices; and relevant characterizations, such as stability, XPS spectra, and conductivity (PDF)

■ AUTHOR INFORMATION

Corresponding Authors

Jun Mei − *Chengdu Development Center of Science and Technology, China Academy of Engineering Physics, Chengdu, Sichuan 610000, China*; Email: meijun12@126.com

Yiying Zhao − *Institute of Materials, China Academy of Engineering Physics, Jiangyou, Sichuan 621908, China*; orcid.org/0000-0002-1424-2516; Email: zhaoyiying@caep.cn

Authors

Yang Liu − *Institute of Materials, China Academy of Engineering Physics, Jiangyou, Sichuan 621908, China; Chengdu Development Center of Science and Technology, China Academy of Engineering Physics, Chengdu, Sichuan 610000, China*

Hao Sun − *Institute of Materials, China Academy of Engineering Physics, Jiangyou, Sichuan 621908, China; Center for Optoelectronics Materials and Devices, Department of Physics, Zhejiang Sci-Tech University, Hangzhou 310018, China*

Feiyi Liao − *Institute of Materials, China Academy of Engineering Physics, Jiangyou, Sichuan 621908, China*

Gaocai Li − *Institute of Materials, China Academy of Engineering Physics, Jiangyou, Sichuan 621908, China; Chengdu Development Center of Science and Technology, China Academy of Engineering Physics, Chengdu, Sichuan 610000, China*

Chen Zhao − *Institute of Materials, China Academy of Engineering Physics, Jiangyou, Sichuan 621908, China*

Can Cui − *Center for Optoelectronics Materials and Devices, Department of Physics, Zhejiang Sci-Tech University, Hangzhou 310018, China*; orcid.org/0000-0002-8429-5875

Complete contact information is available at:
https://pubs.acs.org/10.1021/acsomega.1c04685

Notes
The authors declare no competing financial interest.

■ REFERENCES

(1) Kojima, A.; Teshima, K.; Shirai, Y.; Miyasaka, T. Organometal halide perovskites as visible-light sensitizers for photovoltaic cells. *J. Am. Chem. Soc.* **2009**, *131*, 6050−6051.

(2) National Renewable Energy Laboratory (NREL). Best Research-Cell Efficiency Chart. https://www.nrel.gov/pv/assets/pdfs/best-research-cell-efficiencies.20200104.pdf (accessed 2021-11-17).

(3) Grinberg, I.; West, D. V.; Torres, M.; Gou, G.; Stein, D. M.; Wu, L.; Chen, G.; Gallo, E. M.; Akbashev, A. R.; Davies, P. K.; Spanier, J. E.; Rappe, A. M. Perovskite oxides for visible-light-absorbing ferroelectric and photovoltaic materials. *Nature* **2013**, *503*, 509−512.

(4) Hao, F.; Stoumpos, C. C.; Liu, Z.; Chang, R. P.; Kanatzidis, M. G. Controllable perovskite crystallization at a gas-solid interface for hole conductor-free solar cells with steady power conversion efficiency over 10%. *J. Am. Chem. Soc.* **2014**, *136*, 16411−16419.

(5) Koh, T. M.; Fu, K.; Fang, Y.; Chen, S.; Sum, T. C.; Mathews, N.; Mhaisalkar, S. G.; Boix, P. P.; Baikie, T. Formamidinium-Containing Metal-Halide: An Alternative Material for Near-IR Absorption Perovskite Solar Cells. *J. Phys. Chem. C* **2014**, *118*, 16458−16462.

(6) Shi, X.; Ding, Y.; Zhou, S.; Zhang, B.; Cai, M.; Yao, J.; Hu, L.; Wu, J.; Dai, S.; Nazeeruddin, M. K. Enhanced Interfacial Binding and Electron Extraction Using Boron-Doped TiO 2 for Highly Efficient Hysteresis-Free Perovskite Solar Cells. *Adv. Sci.* **2019**, *6*, 1901213.

(7) Peng, J.; Khan, J.I.; Liu, W.; Ugur, E.; Duong, T.; Wu, Y.; Shen, H.; Wang, K.; Dang, H.; Aydin, E.; et al. A Universal Double-Side Passivation for High Open-Circuit Voltage in Perovskite Solar Cells: Role of Carbonyl Groups in Poly(methyl methacrylate). *Adv. Energy Mater.* **2018**, *8*, 1801208.

(8) Hou, M.; Zhang, H.; Wang, Z.; Xia, Y.; Chen, Y.; Huang, W. Enhancing Efficiency and Stability of Perovskite Solar Cells via a Self-Assembled Dopamine Interfacial Layer. *ACS Appl. Mater. Interfaces* **2018**, *10*, 30607−30613.

(9) Wang, R.; Xue, J.; Wang, K.-L.; Wang, Z.-K.; Luo, Y.; Fenning, D.; Xu, G.; Nuryyeva, S.; Huang, T.; Zhao, Y.; Yang, J. L.; Zhu, J.; Wang, M.; Tan, S.; Yavuz, I.; Houk, K. N.; Yang, Y. Constructive molecular configurations for surface-defect passivation of perovskite photovoltaics. *Science* **2019**, *366*, 1509−1513.

(10) Zhou, Q.; Gao, Y.; Cai, C.; Zhang, Z.; Xu, J.; Yuan, Z.; Gao, P. Dually-Passivated Perovskite Solar Cells with Reduced Voltage Loss and Increased Super Oxide Resistance. *Angew. Chem., Int. Ed.* **2021**, *60*, 8303.

(11) Chen, N.; Yi, X.; Zhuang, J.; Wei, Y.; Zhang, Y.; Wang, F.; Cao, S.; Li, C.; Wang, J. An Efficient Trap Passivator for Perovskite Solar Cells: Poly(propylene glycol) bis(2-aminopropyl ether). *Nano-Micro Lett.* **2020**, *12*, 177.

(12) Cai, Y.; Cui, J.; Chen, M.; Zhang, M.; Han, Y.; Qian, F.; Zhao, H.; Yang, S.; Yang, Z.; Bian, H.; Wang, T.; Guo, K.; Cai, M.; Dai, S.; Liu, Z.; Liu, S. Multifunctional Enhancement for Highly Stable and Efficient Perovskite Solar Cells. *Adv. Funct. Mater.* **2021**, *31*, 2005776.

(13) Li, W.; Dong, H.; Guo, X.; Li, N.; Li, J.; Niu, G.; Wang, L. Graphene oxide as dual functional interface modifier for improving wettability and retarding recombination in hybrid perovskite solar cells. *J. Mater. Chem. A* **2014**, *2*, 20105−20111.

(14) Wang, F.; Geng, W.; Zhou, Y.; Fang, H.-H.; Tong, C.-J.; Loi, M. A.; Liu, L.-M.; Zhao, N. Phenylalkylamine Passivation of Organolead Halide Perovskites Enabling High-Efficiency and Air-Stable Photovoltaic Cells. *Adv. Mater.* **2016**, *28*, 9986−9992.

(15) Zuo, L.; Guo, H.; deQuilettes, D. W.; Jariwala, S.; De Marco, N.; Dong, S.; DeBlock, R.; Ginger, D. S.; Dunn, B.; Wang, M. K.; Yang, Y. Polymer-modified halide perovskite films for efficient and stable planar heterojunction solar cells. *Sci. Adv.* **2017**, *3*, No. e1700106.

(16) Lee, S.; Park, J. H.; Lee, B. R.; Jung, E. D.; Yu, J. C.; Di Nuzzo, D.; Friend, R. H.; Song, M. H. Amine-Based Passivating Materials for Enhanced Optical Properties and Performance of Organic-Inorganic Perovskites in Light-Emitting Diodes. *J. Phys. Chem. Lett.* **2017**, *8*, 1784−1792.

(17) Chen, B.; Rudd, P. N.; Yang, S.; Yuan, Y.; Huang, J. Imperfections and their passivation in halide perovskite solar cells. *Chem. Soc. Rev.* **2019**, *48*, 3842−3867.

(18) Bi, C.; Zheng, X.; Chen, B.; Wei, H.; Huang, J. Spontaneous Passivation of Hybrid Perovskite by Sodium Ions from Glass Substrates: Mysterious Enhancement of Device Efficiency Revealed. *ACS Energy Lett.* **2017**, *2*, 1400−1406.

(19) Abdi-Jalebi, M.; Andaji-Garmaroudi, Z.; Cacovich, S.; Stavrakas, C.; Philippe, B.; Richter, J. M.; Alsari, M.; Booker, E. P.;

Hutter, E. M.; Pearson, A. J.; Lilliu, S.; Savenije, T. J.; Rensmo, H.; Divitini, G.; Ducati, C.; Friend, R. H.; Stranks, S. D. Maximizing and stabilizing luminescence from halide perovskites with potassium passivation. *Nature* **2018**, *555*, 497−501.

(20) Kubicki, D. J.; Prochowicz, D.; Hofstetter, A.; Zakeeruddin, S. M.; Grätzel, M.; Emsley, L. Phase Segregation in Cs-, Rb- and K-Doped Mixed-Cation (MA)x(FA)1-xPbI3 Hybrid Perovskites from Solid-State NMR. *J. Am. Chem. Soc.* **2017**, *139*, 14173−14180.

(21) Song, Z.; Zhao, C.; Liao, F.; Zhao, Y. Perovskite-Betavoltaic Cells: A Novel Application of Organic-Inorganic Hybrid Halide Perovskites. *ACS Appl. Mater. Interfaces* **2019**, *11*, 32969−32977.

(22) Abdi-Jalebi, M.; Dar, M. I.; Sadhanala, A.; Senanayak, S. P.; Franckevičius, M.; Arora, N.; Hu, Y.; Nazeeruddin, M. K.; Zakeeruddin, S. M.; Grätzel, M.; Friend, R. H. Impact of Monovalent Cation Halide Additives on the Structural and Optoelectronic Properties of CH3NH3PbI3Perovskite. *Adv. Energy Mater.* **2016**, *6*, 1502472.

(23) Saliba, M.; Matsui, T.; Domanski, K.; Seo, J.-Y.; Ummadisingu, A.; Zakeeruddin, S. M.; Correa-Baena, J.-P.; Tress, W. R.; Abate, A.; Hagfeldt, A.; Grätzel, M. Incorporation of rubidium cations into perovskite solar cells improves photovoltaic performance. *Science* **2016**, *354*, 206−209.

(24) Zhao, T.; Chueh, C.-C.; Chen, Q.; Rajagopal, A.; Jen, A. K.-Y. Defect Passivation of Organic-Inorganic Hybrid Perovskites by Diammonium Iodide toward High-Performance Photovoltaic Devices. *ACS Energy Lett.* **2016**, *1*, 757−763.

(25) Jokar, E.; Chien, C.-H.; Fathi, A.; Rameez, M.; Chang, Y.-H.; Diau, E. W.-G. Slow surface passivation and crystal relaxation with additives to improve device performance and durability for tin-based perovskite solar cells. *Energy Environ. Sci.* **2018**, *11*, 2353−2362.

(26) Lin, Y.; Bai, Y.; Fang, Y.; Chen, Z.; Yang, S.; Zheng, X.; Tang, S.; Liu, Y.; Zhao, J.; Huang, J. Enhanced Thermal Stability in Perovskite Solar Cells by Assembling 2D/3D Stacking Structures. *J. Phys. Chem. Lett.* **2018**, *9*, 654−658.

(27) Wang, Z.; Lin, Q.; Chmiel, F. P.; Sakai, N.; Herz, L. M.; Snaith, H. J. Efficient ambient-air-stable solar cells with 2D-3D hetero-structured butylammonium-caesium-formamidinium lead halide per-ovskites. *Nat. Energy* **2017**, *2*, 17135.

(28) Pool, V. L.; Gold-Parker, A.; McGehee, M. D.; Toney, M. F. Chlorine in PbCl2-Derived Hybrid-Perovskite Solar Absorbers. *Chem. Mater.* **2015**, *27*, 7240−7243.

(29) Wang, Y.; Wu, T.; Barbaud, J.; Kong, W.; Cui, D.; Chen, H.; Yang, X.; Han, L. Stabilizing heterostructures of soft perovskite semiconductors. *Science* **2019**, *365*, 687−691.

(30) Chen, H.; Liu, T.; Zhou, P.; Li, S.; Ren, J.; He, H.; Wang, J.; Wang, N.; Guo, S. Efficient Bifacial Passivation with Crosslinked Thioctic Acid for High-Performance Methylammonium Lead Iodide Perovskite Solar Cells. *Adv. Mater.* **2020**, *32*, 1905661.

(31) Cao, W.; Zhang, J.; Lin, K.; Qiu, L.; Li, J.; Dong, Y.; Wang, J.; Xia, D.; Fan, R.; Yang, Y. Enhanced Charge Transport and Interface Passivation in Efficient Perovskite Solar Cells Using Sulfur-Doped Graphite Carbon Nitride-Modified SnO 2 -Based Electron Transport Layers. *Sol. RRL* **2021**, *5*, 2100058.

(32) Sun, H.; Xie, D.; Song, Z.; Liang, C.; Xu, L.; Qu, X.; Yao, Y.; Li, D.; Zhai, H.; Zheng, K.; Cui, C.; Zhao, Y. Interface Defects Passivation and Conductivity Improvement in Planar Perovskite Solar Cells Using Na2S-Doped Compact TiO2 Electron Transport Layers. *ACS Appl. Mater. Interfaces* **2020**, *12*, 22853−22861.

(33) Alias, N.; Ali Umar, A.; Malek, N. A. A.; Liu, K.; Li, X.; Abdullah, N. A.; Rosli, M. M.; Abd Rahman, M. Y.; Shi, Z.; Zhang, X.; Zhang, H.; Liu, F.; Wang, J.; Zhan, Y. Photoelectrical Dynamics Uplift in Perovskite Solar Cells by Atoms Thick 2D TiS2 Layer Passivation of TiO2 Nanograss Electron Transport Layer. *ACS Appl. Mater. Interfaces* **2021**, *13*, 3051−3061.

(34) National Institute of Standards and Technology (NIST). X-ray Photoelectron Spectroscopy Database. http://srdata.nist.gov/xps/ (accessed 2021-09-15).

(35) Yang, Z.-Z.; Wang, H.-Y.; Lu, L.; Wang, C.; Zhong, X.-B.; Wang, J.-G.; Jiang, Q.-C. Hierarchical TiO2 spheres as highly efficient polysulfide host for lithium-sulfur batteries. *Sci. Rep.* **2016**, *6*, 22990.

(36) Nowotny, M. K.; Sheppard, L. R.; Bak, T.; Nowotny, J. Defect Chemistry of Titanium Dioxide. Application of Defect Engineering in Processing of TiO2-Based Photocatalysts. *J. Phys. Chem. C* **2008**, *112*, 5275.

(37) Lee, D. S.; Yun, J. S.; Kim, J.; Soufiani, A. M.; Chen, S.; Cho, Y.; Deng, X.; Seidel, J.; Lim, S.; Huang, S.; Ho-Baillie, A. W. Y. Passivation of Grain Boundaries by Phenethylammonium in Formamidinium-Methylammonium Lead Halide Perovskite Solar Cells. *ACS Energy Lett.* **2018**, *3*, 647−654.

(38) Grancini, G.; Roldán-Carmona, C.; Zimmermann, I.; Mosconi, E.; Lee, X.; Martineau, D.; Narbey, S.; Oswald, F.; De Angelis, F.; Graetzel, M.; Nazeeruddin, M. K. One-Year stable perovskite solar cells by 2D/3D interface engineering. *Nat. Commun.* **2017**, *8*, 15684.

(39) Bi, C.; Wang, Q.; Shao, Y.; Yuan, Y.; Xiao, Z.; Huang, J. Non-wetting surface-driven high-aspect-ratio crystalline grain growth for efficient hybrid perovskite solar cells. *Nat. Commun.* **2015**, *6*, 7747.

(40) Chen, J.; Xu, J.; Xiao, L.; Zhang, B.; Dai, S.; Yao, J. Mixed-Organic-Cation (FA)x(MA)1-xPbI3 Planar Perovskite Solar Cells with 16.48% Efficiency via a Low-Pressure Vapor-Assisted Solution Process. *ACS Appl. Mater. Interfaces* **2017**, *9*, 2449−2458.

(41) Bube, R. H.; Richard, H. Trap Density Determination by Space-Charge-Limited Currents. *J. Appl. Phys.* **1962**, *33*, 1733−1737.

(42) Ren, Y.-K.; Ding, X.-H.; Wu, Y.-H.; Zhu, J.; Hayat, T.; Alsaedi, A.; Xu, Y.-F.; Li, Z.-Q.; Yang, S.-F.; Dai, S.-Y. Temperature-assisted rapid nucleation: a facile method to optimize the film morphology for perovskite solar cells. *J. Mater. Chem. A* **2017**, *5*, 20327−20333.